Available online at www.sciencedirect.com

SCIENCE DIRECT

Cement and Concrete Research 35 (2005) 384–392

CEMENT AND CONCRETE RESEARCH

Experimental and theoretical investigation on the postcracking inelastic behavior of synthetic fiber reinforced concrete beams

Byung Hwan Oh*, Dae Gyun Park, Ji Cheol Kim, Young Cheol Choi

Department of Civil Engineering, Seoul National University, San 56-1, Shinrim-dong, Gwanak-ku, Seoul 151-742, Korea

Received 24 February 2004; accepted 12 July 2004

Abstract

A realistic method of analysis for the postcracking behavior of newly developed structural synthetic fiber reinforced concrete beams is proposed. In order to predict the postcracking behavior, pullout behavior of single fiber is identified by tests and employed in the model in addition to the realistic stress–strain behavior of concrete in compression and tension. A probabilistic approach is used to calculate the effective number of fibers across the crack faces and to calculate the probability of nonpullout failure of fibers. The proposed theory is compared with test data and shows good agreement. The proposed theory can be efficiently used to predict the load–deflection behavior, moment–curvature relation, load–crack mouth opening displacement (CMOD) relation of synthetic fiber reinforced concrete beams.

Keywords: Fiber reinforcement; Microcracking; Pullout strength; Structural synthetic fiber; Tensile properties

1. Introduction

Fibers have been used in many applications, including tunnel linings, impact-resistant structures, and repair/rehabilitation of damaged structures. However, the most important application of fibers would be to prevent or control the tensile cracking occurring in concrete structures [1–13]. It is, therefore, necessary to realistically model the postcracking behavior of fiber-reinforced concrete (FRC) members.

Recently, structurally efficient synthetic fibers have been developed by authors and coworkers [10]. Here, structural synthetic fibers mean that they exhibit structurally effective properties, such as increase of toughness and/or loading carrying capacity after cracking. These synthetic fibers have advantages compared to steel or other fibers in that they are corrosion-resistant and exhibit high energy-absorption capacity.

The purpose of the present study is to explore experimentally and theoretically the cracking resistance and postcracking behavior of newly developed structural synthetic fiber reinforced concrete beams. To this end, the pullout tests of fibers were conducted which simulate pullout behavior of fibers at crack surfaces. The arbitrarily oriented fibers at the crack surface have been considered by introducing a probabilistic concept. The load–deflection and moment–curvature curves were generated from the theory derived in this study and compared with test data.

2. Models for postcracking behavior

2.1. Concept of analysis

A fiber-reinforced concrete beam as shown in Fig. 1 has been considered for the analysis of postcracking behavior. Fig. 1 shows the failure mode of a beam with the crack mouth opening displacement (CMOD). Fig. 2 depicts the strain and stress distributions along the depth of normal reinforced concrete (RC) beam. These stress distributions can be redrawn as shown in Fig. 3 for fiber-reinforced concrete (FRC) beams. In Fig. 3, the pullout forces of fibers in tensile region depend on the crack opening displacements along the depth from neutral axis.

* Corresponding author. Tel.: +82 2 880 7350; fax: +82 2 887 0349.
E-mail address: bhohcon@snu.ac.kr (B. Hwan Oh).

0008-8846/$ - see front matter © 2004 Elsevier Ltd. All rights reserved.
doi:10.1016/j.cemconres.2004.07.019

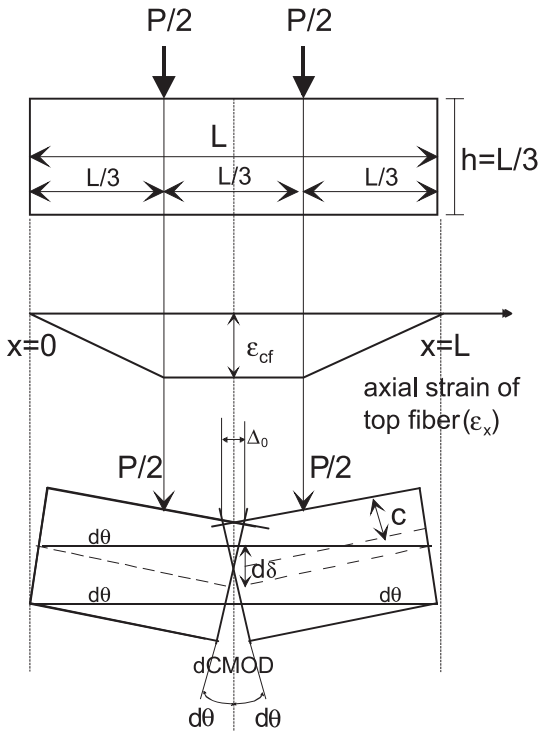

Fig. 1. Failure mode of FRC beam under load.

In order to obtain the postcracking behavior of FRC beams, the stress–strain relations of concrete in compression and tension, and the stress–crack width relation after cracking must be properly defined. This will be clarified in the next section.

The Hognestad's stress–strain relation (Eqs. (1) and (2)) of concrete in compression is employed in this study, which is one of the most generally used equation to model the constitutive behavior of concrete. Fig. 4 exhibits the typical stress–strain relation of concrete in compression [14].

$$f_c = f_c' \left[2\frac{\varepsilon_c}{\varepsilon_0} - \left(\frac{\varepsilon_c}{\varepsilon_0}\right)^2 \right] \quad \text{for } 0 \le \varepsilon_c \le \varepsilon_0 \tag{1}$$

$$f_c = f_c' \left[1 - \frac{0.15}{0.004 - \varepsilon_0}(\varepsilon_c - \varepsilon_0) \right] \quad \text{for } \varepsilon_0 \le \varepsilon_c \le 0.003 \tag{2}$$

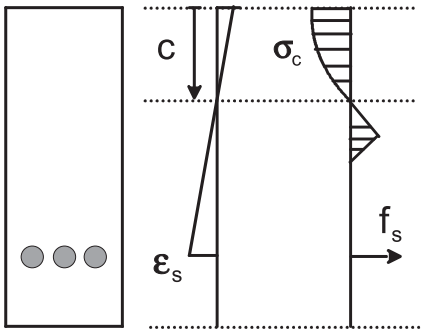

Fig. 2. Stress and strain relation of RC beam.

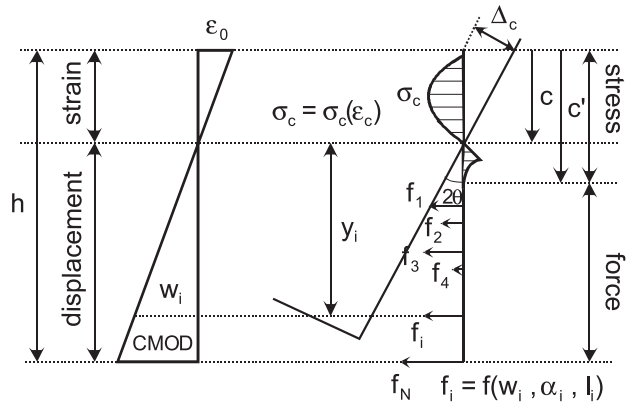

Fig. 3. Schematic view of forces and stresses acting on cracked section of FRC beam.

in which f_c' =compressive strength of concrete and ε_0=the strain at peak stress (see Fig. 4). The force C in compression zone can be written as follows.

$$C = \alpha f_c' \, bc \tag{3}$$

where α=the factor for average stress, b=width of beam, and c=the depth of neutral axis from the top face of a beam. The factor α can be considered as a conversion factor from actual stress–strain curves to a rectangular stress block. This can be obtained by equating the area under actual stress–strain curve to the area under rectangular stress block as follows [14].

$$\int_0^{\varepsilon_{cf}} f_c d\varepsilon_c = \alpha f_c' \, \varepsilon_{cf}; \qquad \text{Then } \alpha = \frac{\int_0^{\varepsilon_{cf}} f_c d\varepsilon_c}{f_c' \, \varepsilon_{cf}} \tag{4}$$

The location of the compression force, γc, from the top fiber can be obtained as

$$\gamma = 1 - \frac{\int_0^{\varepsilon_{cf}} \varepsilon_c f_c d\varepsilon_c}{\varepsilon_{cf} \int_0^{\varepsilon_{cf}} f_c d\varepsilon_c} \tag{5}$$

where γ=centroid factor for compression force.

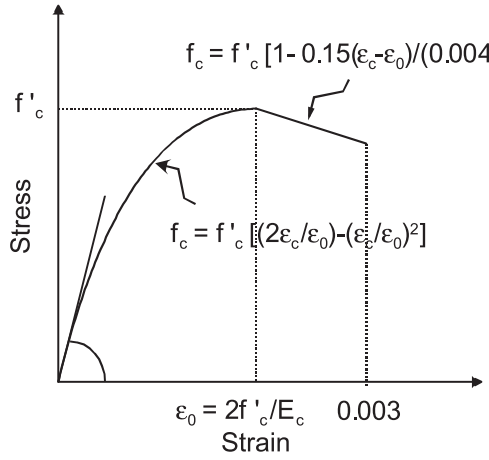

Fig. 4. Hongnestad's stress–strain curve for concrete in compression.

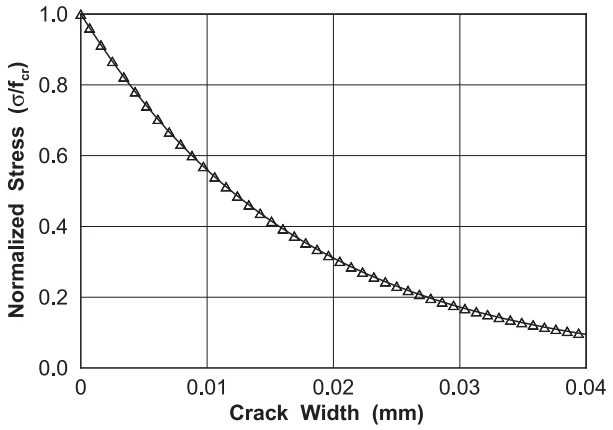

Fig. 5. Tension softening curve after cracking (Shah's model).

2.2. Behavior of concrete in tension before crack occurrence

The tensile behavior of concrete can be reasonably assumed as linear elastic before cracking. The elastic modulus is generally described as [1]

$$E_{ct} = 5500\sqrt{f_c'} \ \text{(MPa)} \tag{6}$$

2.3. Postcracking behavior of concrete after tensile strength

The cracking starts to occur right after the tensile stress reaches the tensile strength and the tensile stress decreases as the crack width increases. The strain at first cracking, ε_{cr}, can be obtained as follows.

$$\varepsilon_{cr} = \frac{f_r}{E_{ct}} \tag{7}$$

in which f_r=tensile strength of concrete, E_{ct}=elastic modulus before cracking.

The stresses after cracking depend on the widths of cracks. It is reasonably written here based on the Gopalotratnam and Shah's [15] model [see Fig. 5].

$$\frac{\sigma_{ct}}{f_c} = e^{-kw^{\lambda}} \tag{8}$$

in which σ_{ct}=the tensile stresses after cracking, k=empirical constant=60.8, w=crack width (in mm), λ=empirical constant=1.01.

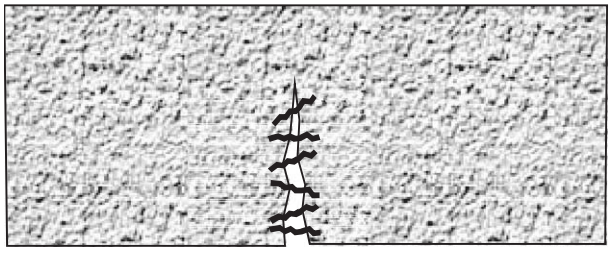

Fig. 6. Orientation and embedded length of randomly distributed fibers.

Table 1
Average number of fibers according to fiber content

Fiber content, percent of volume	0.75%	1.50%
Average, fibers per 4 cm^2	7.922	15.173
Standard deviation, fibers per 4 cm^2	6	8.9
Sample size, n	448	493

2.4. Calculation of sectional forces and deflections of FRC beams

The deformation of concrete beams without reinforcing bars is usually localized at central position as shown in Fig. 1. The cracked portion at central location acts as a plastic hinge. The distribution of compressive strain at extreme fiber of the beam, ε_x, is shown in Fig. 1(b). The displacement Δ_n at compression face can be obtained from this compressive strain distribution ε_x.

$$\Delta_0 = \int_0^L \varepsilon_x \mathrm{d}x = \varepsilon_{cf}\frac{2}{3}L \tag{9}$$

The slope (rotation angle) of beam, $\mathrm{d}\theta$, may also be obtained from Fig. 1.

$$\mathrm{d}\theta \approx \frac{\Delta_0}{2c} \tag{10}$$

The deflection at central position is obtained from the slope of the beam as follows.

$$\mathrm{d}\delta = \mathrm{d}\theta\frac{L}{2} \tag{11}$$

The crack mouth opening displacement (CMOD) at the bottom surface is also written as

$$\mathrm{dCMOD} = 2[\mathrm{d}\theta(h-c)] \tag{12}$$

The internal resisting moment, M_e, of the beam can be derived from the stress distributions of concrete in compression and tension zones and also the pullout forces of all the fibers across the crack plane as shown in Fig. 3 (Eqs. (13) and (14)).

$$\int_0^c \sigma_c(b\mathrm{d}y) + \sum_{i=1}^{N} f_i = 0 \tag{13}$$

$$M_e = \int_0^c \sigma_c b\mathrm{d}yy + \sum_{i=1}^{N}(f_i y_i) \tag{14}$$

From the moment of Eq. (14), the applied load on the beam, P, is obtained as follows.

$$P = \frac{6M_e}{L} \tag{15}$$

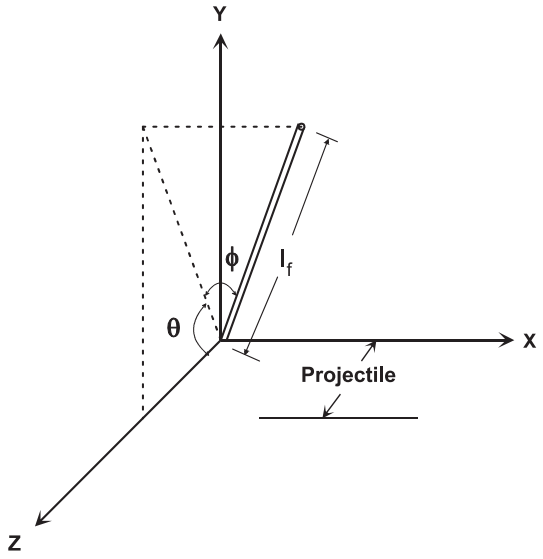

Fig. 7. Three-dimensional fiber orientation.

The pullout force f_i of the fiber of ith layer in Eq. (14) should be obtained from the relation of bond stress and bond slip of a fiber and they directly depend on the crack widths of the beam (see Eq. (16)).

$$w_i = \left[\frac{\mathrm{CMOD}}{(h-c)}\right] y_i \tag{16}$$

The fibers are randomly distributed at the crack plane as shown in Fig. 6 and this effect must be considered appropriately to calculate the fiber forces. Banthia and Trottier [2] reported that the average number of fibers per unit area of crack plane follows normal distribution and can be summarized depending on the fiber contents as shown in Table 1.

On the other hand, Soroushian and Lee [12 13] proposed the number of fibers per unit area, N_1, as follows.

$$N_1 = \alpha \frac{V_f}{A_f} \tag{17}$$

where α=fiber orientation factor, V_f=fiber content, and A_f=cross-sectional area of fibers.

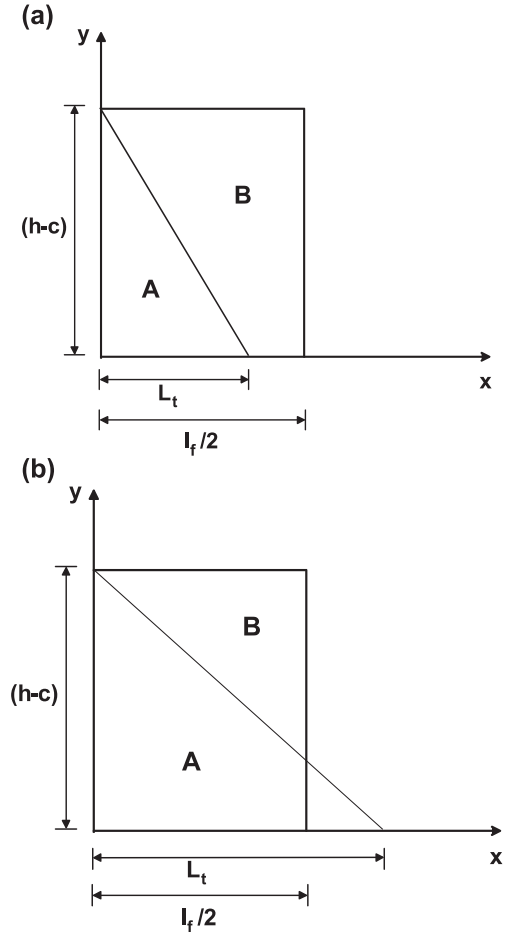

Fig. 9. (a) Relation between required anchorage and half of fiber length ($L_f \le 1/2l_f$). (b) Relation between required anchorage and half of fiber length ($L_f > 1/2l_f$).

The orientation factor α can be considered as the effective factor that an arbitrarily oriented fiber is perpendicular to the crack plane (see Fig. 7).

$$\alpha_0 = \frac{\int_0^{\frac{\pi}{2}} \int_0^{\frac{\pi}{2}} l_f \cos\theta \cos\psi \, d\theta \, d\psi}{\left(\frac{\pi}{2}\right)^2 l_f} = 0.405 \tag{18}$$

If the boundary of the structure restrains the arbitrary orientation of the fibers, the orientation factor for a specified

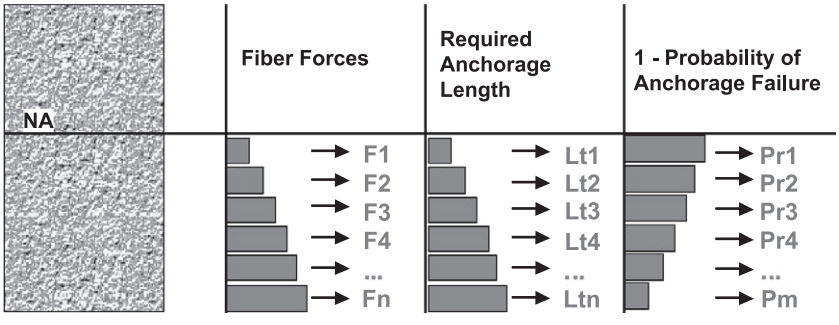

Fig. 8. Fiber force, required anchorage length, and probability of nonanchorage failure.

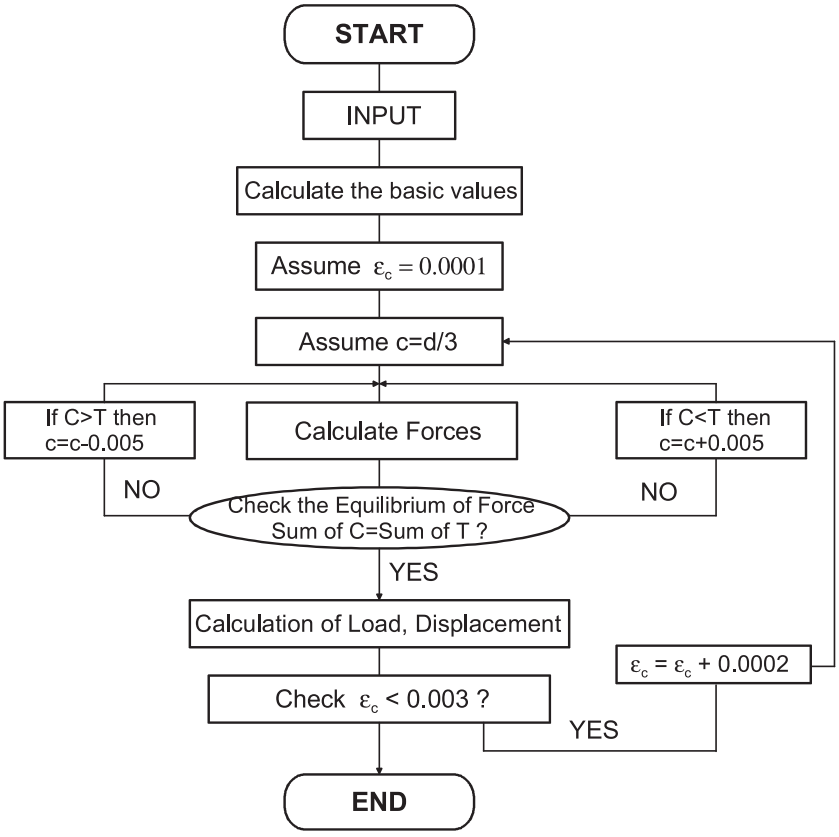

Fig. 10. Flowchart for structural analysis.

direction becomes larger. Soroushian and Lee [12,13] reported the orientation factor for two-side-restrained case as follows.

$$\alpha_1 = \frac{\int_{d_f/2}^{h/2} \beta_1 \mathrm{d}y}{h/2} \quad \text{for } h<l_f \tag{19}$$

$$\alpha_1 = \frac{l_f \int_{d_f/2}^{l_f/2} \beta_1 \mathrm{d}y}{h l_f/2} + 0.405\left(1 - l_f/h\right) \tag{20}$$

$$\text{where } \beta_1 = \frac{\int_0^{\pi/2} \int_{r_0}^{r} l_f \cos\theta \cos\psi \mathrm{d}\theta \mathrm{d}\psi}{l_f(\pi/2)r} \tag{21}$$

$$\text{with } r_0 = \sin^{-1}\left(d_f/l_f\right) \text{ and } r = \sin^{-1}\left(2y/l_f\right) \tag{22}$$

The tensile force (F_i) resisted by fibers at each layer of tensile zone of the beam can be obtained by multiplying the fiber force f_i of that layer by the number of fibers. The force f_i of single fiber can be derived from the bond stress–slip relation, which is also dependent upon the crack width w_i of ith layer (see Fig. 3). This bond stress–slip relation of structural synthetic fiber will be directly obtained by tests, which will be described in the following section.

The development length L_f of a fiber required for not to be pulled out at the crack plane may be derived as shown in Eq. (23).

$$L_t = \frac{f_i}{\Sigma_0 \Gamma_u} \tag{23}$$

in which Σ_0=perimeter of a fiber, and τ_u=bond strength of a fiber. Therefore, the actual embedment length of fibers should be larger than the required development length in order not to be pulled out.

Fig. 8 summarizes the fiber forces, required anchorage lengths, and the probabilities of nonanchorage failure for

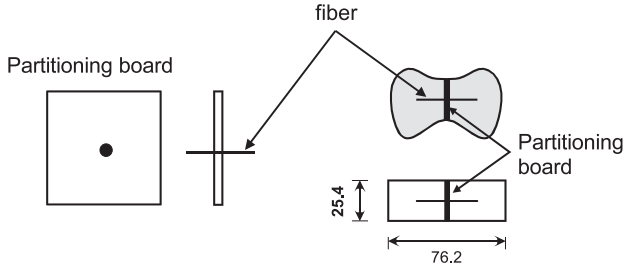

Fig. 11. Pullout test specimen.

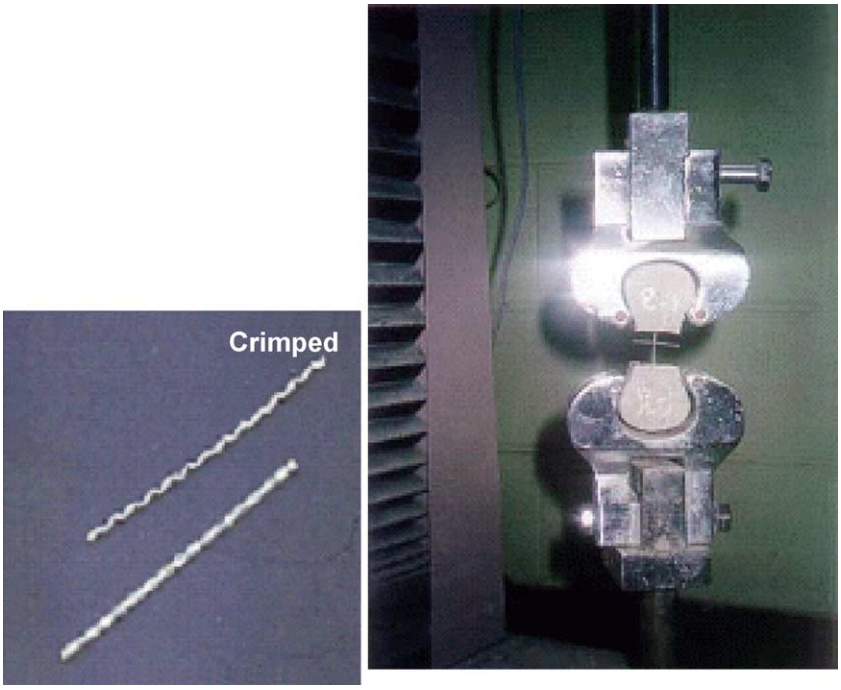

Fig. 12. Photograph of pullout test with crimped fiber.

various layers of cracked section of a beam. The probability of nonanchorage (or nonpullout) failure P_r can be derived as follows by two cases.

(1) Case 1: Required anchorage length ≤ half of fiber length ($L_t \le l_f/2$)

Fig. 9 represents the cracked region of a beam. This is the case that the half of the actual fiber length (the region B in Fig. 9(a)) is larger than the required anchorage length (the region A in Fig. 9(a)). This can be written in a formalized equation as follows.

$$P_r = \frac{\text{area of B}}{\text{total area A and B}} = 1 - \frac{\text{area of A}}{\text{total area A and B}} = 1 - \frac{(h-c)L_t/2}{(h-c)l_f/2} = 1 - \frac{L_f}{l_f} \quad (24)$$

(2) Case 2: Required anchorage length>half of fiber length ($L_t > l_f/2$)

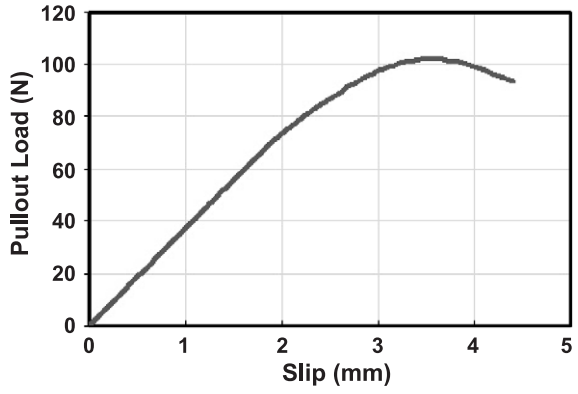

Fig. 13. Load–slip relation for crimped-type synthetic fiber.

This is the case of Fig. 9(b) that the required anchorage length is larger than the half of actual fiber length. This can be expressed as the following equation.

$$P_r = \frac{\text{area of region B}}{\text{total area of rectangle}} = \frac{(l_f/2)k/2}{(h-c)l_f/2} = \frac{1}{2}\frac{l_f/2}{L_t} = \frac{1}{4}\frac{l_f}{L_t} \quad (25)$$

in which $k = \frac{l_f}{2}(h-c)/L_t$ (see Fig. 9).

Finally, the tensile forces resisted by fibers can be obtained from the number of fibers at each layer, effective orientation factor α, and the probability of nonanchorage failure P_r. The flow diagram for the flexural analysis of synthetic fiber reinforced concrete beams is summarized in Fig. 10.

3. Tests for postcracking behavior of structural synthetic fiber reinforced concrete beams

3.1. Pullout test for single fiber

The authors developed recently new structural synthetic fibers which are of crimped type with the length of 50 mm. Fig. 11 shows the pullout test specimen specially prepared for obtaining the pullout load–slip relation. Fig. 12 shows

Table 2
Mixture proportion for test specimens

W/C (%)	Unit weight (kg/m^3)				Fiber content (1%)
	Cement	Water	Sand	Gravel	
45	453	204	1115	487	9

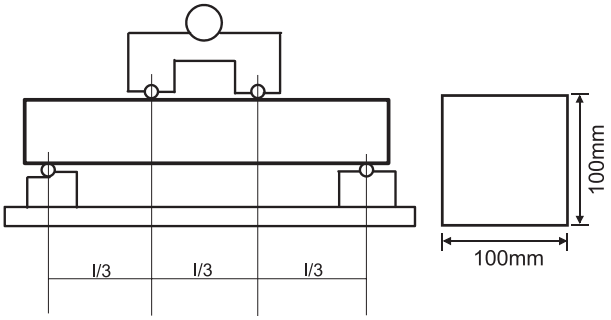

Fig. 14. Schematic view of flexural tests.

the photograph for actual pullout test arrangement with a crimped synthetic fiber. Armelin [16] also conducted a similar pullout study for steel fibers to predict the postcracking performance of steel-fiber-reinforced concrete beams. The same mixtures were used for both pullout tests and FRC beam tests.

Fig. 13 depicts the average pullout load versus slip relation obtained from the present tests. The bond load–slip equation obtained from the tests may have the following form.

$$F_p = \frac{aS}{b + cS^d} \tag{26}$$

where a, b, c, and d are the constants to be obtained from test data, and F_p=pullout load (kN), S=slip (in mm).

3.2. Flexural tests for structural synthetic fiber reinforced concrete beam

The concrete beams reinforced with structural synthetic fibers have been tested to obtain the flexural behavior, including the load–deflection behavior, load–CMOD relations, and moment–curvature relations [17]. The mixture proportion of concrete is summarized in Table 2. The water–cement ratio was 0.45 and the fiber content was 1% of total concrete volume.

The compressive strength was 36 MPa and the flexural strength was 4.8 MPa, respectively.

The mixture was designed to accommodate the use for tunnel shotcrete lining structures.

Fig. 14 exhibits the arrangement for flexural tests of fiber-reinforced concrete beams in a four-point loading condition. Fig. 15 shows the special measuring device for central deflection of the beam. This device allows to measure exact relative displacements between the supports and center point.

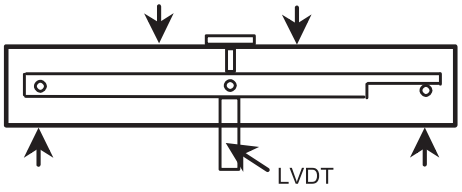

Fig. 15. Devices for displacement measurement.

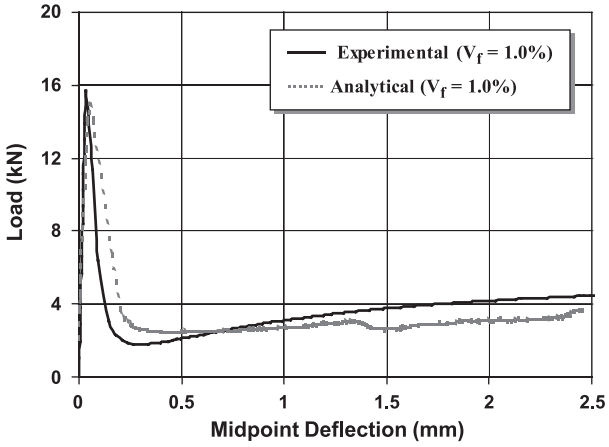

Fig. 16. Load–deflection curve for structural synthetic fiber concrete beam (fiber content: V_f=1.0% by volume).

The dimension of the beam was 100×100×400 mm and the span length was 300 mm. The load was applied in displacement control manner with the rate specified in the static testing standard.

4. Analyses of test results and comparisons with theory

Fig. 16 shows the load–deflection curves obtained from the present tests for the beam with structural synthetic fiber volume of 1%. Fig. 16 also compares the test data with the theory proposed in the previous section. It can be seen that the theoretical predictions fairly well agree with test data even after postcracking ranges.

The salient feature of the postcracking behavior of structural synthetic fiber reinforced concrete beams is that the resisting load drops down right after first cracking, probably due to initial slip of fibers at crack plane, and then starts to increase due to structurally effective synthetic fibers in tensile region. Fig. 17 also exhibits the similar behavior

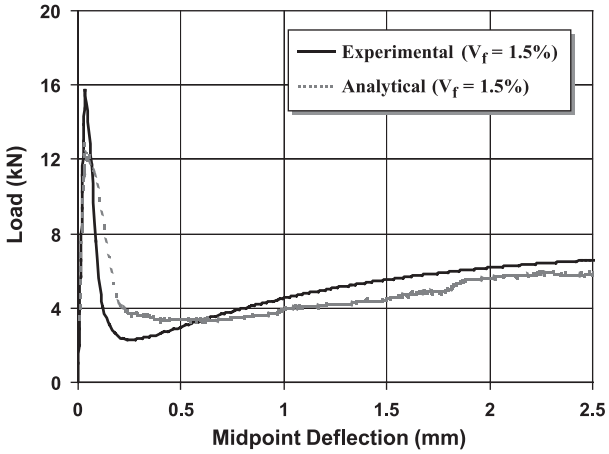

Fig. 17. Load–deflection curve for structural synthetic fiber concrete beam (fiber content: V_f=1.5% by volume).

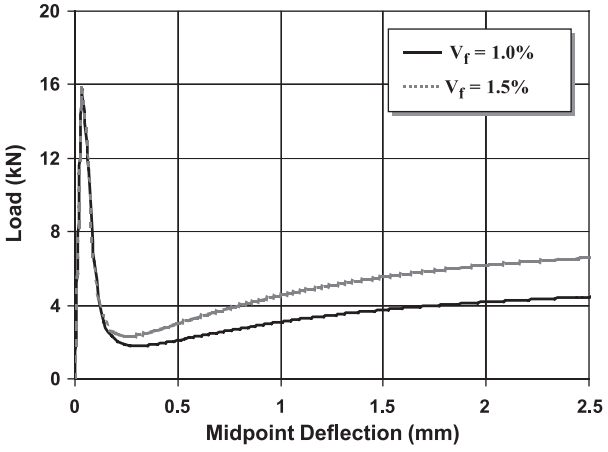

Fig. 18. Effect of fiber content on load and deflection.

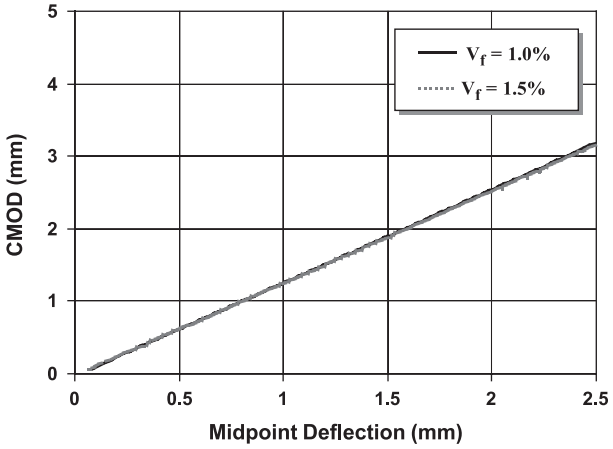

Fig. 20. Relation between CMOD and deflection.

of structural synthetic fiber reinforced concrete beam for fiber volume of 1.5%. It is seen again in Fig. 17 that the proposed theory agrees very well with the measured data, even up to the large deflection of the beam.

Fig. 18 shows the comparison of load–deflection behavior for two different fiber volume contents. Fig. 18 indicates that the FRC beam with larger volume of fiber content (namely, 1.5% by volume) exhibits higher resistance especially after larger deflection.

Fig. 19 describes the load–CMOD relations for two different fiber volume contents. It is noted here that, at the same loads after cracking, the FRC beam with larger volume of fibers exhibits much smaller CMOD values. This is indeed a great beneficial effect of structural synthetic fibers. Fig. 20 shows the relation between CMOD and central deflection of FRC beam. These relations are very much similar for different fiber volume contents. Therefore, this relation of CMOD versus central displacement may be regarded as a material property for structural synthetic fiber reinforced concrete beam.

Fig. 21 shows the change of neutral axis depth according to central deflection. It is seen that the neutral axis depth continuously decreases, which reflects the crack growth according to the increase of applied load. Fig. 22 describes the moment–curvature relations for FRC beams with two different fiber volumes. These curves are very similar to load–deflection curves previously described for synthetic fiber reinforced concrete beams.

5. Conclusions

The postcracking behavior of concrete beams reinforced with recently developed structural synthetic fibers is investigated in the present study. In order to develop a realistic model for postcracking behavior of structural synthetic FRC beams, the randomness of orientation of fibers and the effective number of fibers at the crack plane were first considered and then new concept of the probability of nonpullout failure of fibers at the crack plane was introduced and derived in this study.

In order to calculate the pullout forces of structural synthetic fibers at the crack plane, the pullout tests for fibers

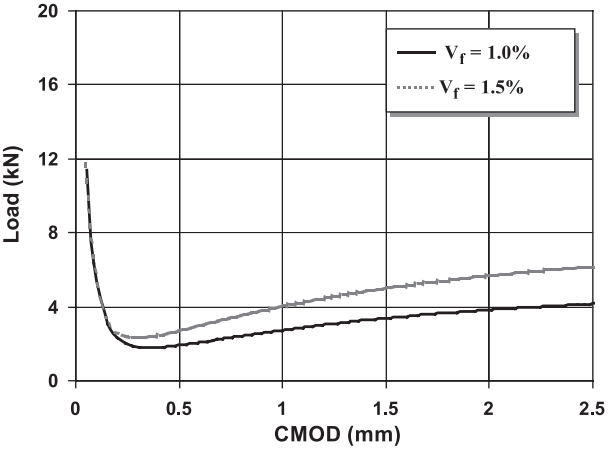

Fig. 19. Effect of fiber content on load–CMOD relation.

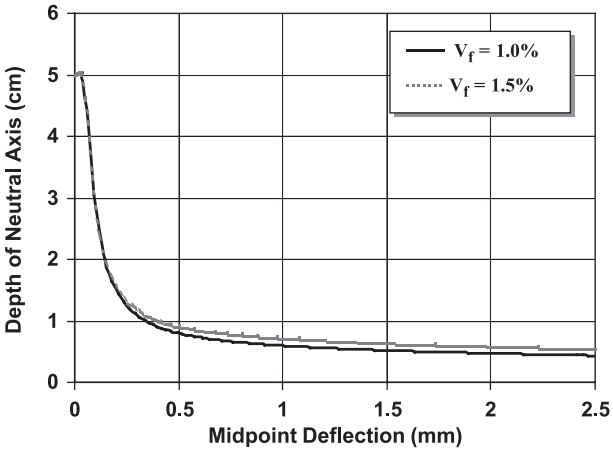

Fig. 21. Variation of neutral axis depth according to the increase of deflection.

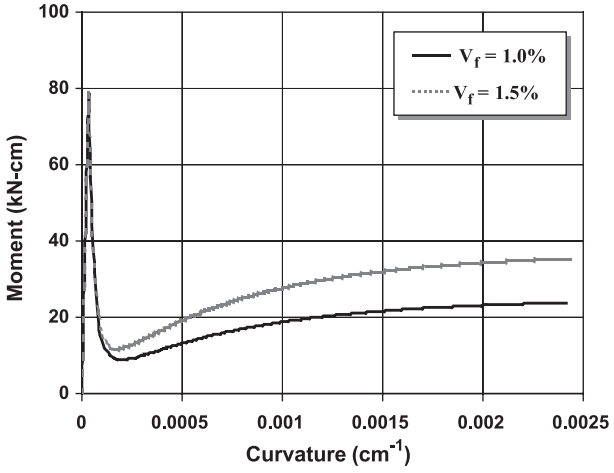

Fig. 22. Prediction of moment and curvature relation.

were also conducted and an appropriate relation between bond forces and slips was derived. All these models were incorporated to formulate a method for flexural analysis of structural synthetic FRC beams.

The present tests for structural synthetic FRC beams indicate that the resisting load drops down right after the peak load and then starts to increase continuously due to the resistance of structural synthetic fibers. The theory developed in this study describes well these phenomena observed in the tests.

The load–CMOD relation, CMOD–deflection, and moment–curvature relation were also reasonably predicted by the proposed theory. The present study indicates that the FRC beams with larger amount of fibers exhibits much smaller CMOD values at the same applied loads, which is one of the great beneficial effects of newly developed structural synthetic fibers. The present study also indicates that the relation between CMODs and central displacements is almost same for the beams with different fiber volumes and, therefore, this relation can be regarded as a material property for structural synthetic fiber reinforced concrete members.

The present study allows more realistic analysis and application of recently developed structural synthetic fiber reinforced concrete beams.

6. Notation

The following symbols are used in this paper

c	Neutral depth of cross section
c'	Depth from the top of cross-section to tensile stress acting on concrete
$\mathrm{d}\delta$	Increment of midpoint deflection
$\mathrm{d}\theta$	Increment of rotation in cracked section
E_{ct}	Elastic modulus of concrete in tensile zone
f_{c}, σ_{c}	Compression stress of concrete
f'_{c}	Compression strength of concrete
f_{cr}	Tensile strength of concrete
f_i	Pullout force of (i)th fiber
F_{t}	Pullout force of total fiber
l_{f}	Length of fiber
L_{t}	Anchorage length between fiber and concrete
V_{f}	Volume fraction of fiber
ε_{c}	Strain of concrete
ε_0	Peak strain of concrete
σ_{ct}	Tensile stress of concrete

Acknowledgements

The financial support from the National Research Laboratory (NRL) Program of Korea is gratefully acknowledged.

References

[1] ACI Committee 544, Design considerations for steel fiber reinforced concrete.
[2] N. Banthia, J. Trottier, Concrete reinforced with deformed steel fibers: Part I. Bond–slip mechanism, ACI Mater. J. 91 (5) (1994) 435–446.
[3] A.S. Ezeldin, P.N. Balaguru, Normal and high strength fiber reinforced concrete under compression, J. Mater. Civ. Eng. 4 (4) (1992) 415–427.
[4] V.S. Goparalatnam, M. Wecharatana, Fracture toughness of fiber reinforced concrete, ACI Mater. J. 88 (4) (1991) 339–353.
[5] D. Lange-Kornbam, B.L. Karihaloo, Tension softening of fibre-reinforced cementitious composites, Cem. Concr. Compos. 19 (1997) 315–328.
[6] C. Leung, Y.P. Geng, Micromechanical modeling of softening behavior in steel fiber reinforced cementitious composites, Int. J. Solids Struct. 35 (1998) 4205–4222.
[7] V.C. Li, et al., Influence of fiber bridging on structural size-effect, Int. J. Solids Struct. 35 (1998) 4223–4238.
[8] M.C. Nataraja, et al., Stress–strain curves for steel-fiber reinforced concrete under compression, Cem. Concr. Compos. 21 (1999) 383–390.
[9] B.H. Oh, Flexural analysis of reinforced concrete beams containing steel fibers, ASCE J. Struct. Eng. 118 (10) (1992) 2691–2698.
[10] B.H. Oh, J.C. Kim, Cracking and flexural behavior of structural synthetic fiber reinforced concrete beams, KCI J. 14 (6) (2003) 900–909.
[11] J.P. Romualdi, J.A. Mandel, Tensile strength of concrete as affected by uniformly distributed and closely spaced short lengths of wire reinforcement, ACI J. 61 (6) (1964) 650–670.
[12] P. Soroushian, C. Lee, Distribution and orientation of fibers in steel fiber reinforced concrete, ACI Mater. J. 87 (5) (1990) 433–439.
[13] P. Soroushian, C. Lee, Tensile strength of steel fiber reinforced concrete: Correlation with some measures of fiber spacing, ACI Mater. J. 87 (5) (1990) 542–546.
[14] R. Park, T. Paulay, Reinforced Concrete Structures, John Wiley and Sons, New York, 1975.
[15] V.S. Gopalaratnam, S.P. Shah, Softening response of plain concrete in direct tension, ACI J. 82 (3) (1985) 310–323.
[16] H. Armelin, et al., Predicting the flexural post-cracking performance of steel-fiber reinforced concrete from the pull-out of single fibers, ACI Mater. J. 94 (1) (1997) 18–31.
[17] ASTM C 1018-89, Standard Test Method for Flexural Toughness and First-Crack Strength of Fiber Reinforced Concrete (Using Beam with Third-Point Loading), ASTM Standards, V. 04.02, ASTM, (1991) 507–513.